Journal of Polymer Research (2022) 29: 427
https://doi.org/10.1007/s10965-022-03216-x

ORIGINAL PAPER

Ex situ synthesis of MOF@PET/cotton textile fibers as potential antibacterial materials

Sergio Alejandro Torres-Cortés[1] · Mauricio Velasquez[2] · León Darío Pérez[1] · César A. Sierra[1]

Received: 1 April 2022 / Accepted: 28 July 2022 / Published online: 14 September 2022

Abstract

There is considerable scientific literature on MOF-based antibacterial textiles, especially with *in situ* methodologies for their synthesis. On the contrary, the *ex situ* synthesis of MOFs on fabrics has been little explored. Although, the latter may have more significant advantages when the expectation is to scale up the process industrially. The present study describes the synthesis of *ex situ* obtained MOF-199 and MOF-UiO-66-NH_2 onto carboxylated polyester/cotton (PETco) textile fibers and their preliminary-qualitative analysis as potential antibacterial textiles. For this, free synthesized MOFs were anchored on a previously carboxylated PETco fiber, using conditions that seek the formation of coordination bonds between the carboxyl groups of the fiber and the metal in the MOF. After soxhlet purification with water and methanol for more than 48 h, analysis by FTIR-ATR and XRD shows the superposition of signals typical of the fiber and the MOF, resembling what was previously reported for cotton-MOF systems. XPS showed 4.47% Cu, with Cu–O-C interactions for MOF-199@PETco, and 12.06% Zr, with Zr-O-C interactions for MOF UiO-66-NH_2@PETco. Results corroborated by the SEM micrographs, which show the expected morphology for MOF-199, and homogeneously distributed MOF UiO-66-NH_2 crystals when they are anchored to the fiber.

Keywords MOF · PET · Cotton · Fibers · *Ex situ* synthesis · Antibacterial textile

Abbreviations

ACN	Acetonitrile
ATCC	American Type Culture Collection
ATRP-ARGET	Atom Transfer Radical Polymerization – Activators ReGenerated by Electron Transfer
BDC	Benzene dicarboxylic
BIBB	2-Bromoisobutiryl bromide
BTC	Benzene tricarboxylic
DMAP	4-Dimethylaminopyridine
DMF	Dimethylformamide
DMSO	Dimethyl sulfoxide
EDX	Energy Dispersive X-Ray Spectroscopy
FTIR-ATR	Fourier-Transformed Infrared Spectroscopy – Attenuated Total Reflectance
MAA	Methacrylic acid
MOF	Metal-Organic Framework
PETco	Polyethylene terephthalate/cotton
PMDETA	*N,N,N',N'',N''*-Pentamethyldiethyilene-triamine
PXRD	Powder X-Ray Diffraction
SEM	Scanning Electron Microscopy
TEA	*N,N,N*-Triethylamine
UiO	Universitet i Oslo
UV	Ultraviolet
XPS	X-Ray Photoelectron Spectroscopy

✉ César A. Sierra
casierraa@unal.edu.co

[1] Grupo de Investigación en Macromoléculas, Departamento de Química, Facultad de Ciencias, Universidad Nacional de Colombia, Kra. 30 No. 45-03, Bogotá 11001, Colombia

[2] Departamento de Química, Facultad de Ciencias, Estado Sólido Y Catálisis Ambiental (ESCA), Universidad Nacional de Colombia, Kra 30 No. 45-03, Bogotá 11001, Colombia

Introduction

Metal–organic Frameworks (MOFs) are organic–inorganic reticular polymers composed of metallic clusters in coordination structures known as secondary building units (SBU), bonded by organic linkers. Since Hoskins and Robson published the first

tridimensional coordination reticular arrangements [1, 2], the number of publications with their interesting physicochemical properties [3–6] and prominent applications has grown exponentially in both importance and number [7–17].

Nevertheless, because of their fragility and fine crystalline powder form that causes the leaching and loss of metallic centers, MOFs' industrial incorporation into several applications have been very difficult [18]. One way to solve the above is the generation of composite materials where MOFs are physically or chemically bonded to a solid surface, e.g., textile fibers, where MOFs are expected to increase their operational stability due to the barrier given by the surface where it is anchored. Cotton is the most broadly used textile fiber for MOF immobilization due mainly to its excellent bioavailability and biocompatibility. Properties that, together with the widely studied antibacterial activity of various MOFs, have enabled the development of antibacterial textiles [19–21]. With the appropriate physical and chemical treatments, the surface of cellulosic fibers can lead to several types of functional agents, either through leaching or non-leaching modifications. Treatments that have a wide range of applications ranging from UV protection, flame retardants, water remediation, and, as in this case, antibacterial finishing on garments [22]. Where for this last application, the use of quaternary ammonium compounds, polyguanides, N-halamines, triclosan, chitosan, plant extracts, or essential oils of plants (aloe vera, eugenol, alkaloids, saponins, among other natural products) stands out, and nanoparticles of metals and metal oxides such as Ag or CuO. Materials that function as finishes on cotton showing considerable stability and biocompatibility, thus being the most used to impart antibacterial properties in textiles [23]. However, these materials commonly used for antibacterial textile finishing have significant disadvantages: some of them are difficult and expensive to obtain from natural sources (such as essential oils), and they present significant environmental risks for aquatic species due to their toxicity (e.g., Ag nanoparticles and triclosan), can develop bacterial or fungal resistance, or can be chemically deactivated as quaternary ammonium cationic salts, which, when encountering anionic species, are electrically neutralized [24–27]. Difficulties that have led researchers to explore new antibacterial materials that are cheaper, easier to obtain, and safer, such as MOFs. Materials that have shown significant biocompatibility, low toxicity, great efficacy against nosocomial bacteria and fungi, and little or no resistance to their effect.

In 2012, Abbasi [28] and Abbasi et al. [29] reported one of the first textile/MOF materials, a coating of MOF-199 onto silk fibers that showed antimicrobial activity against *E. coli*. and *S. aureus*. In 2014, Hinestroza et al. [30] suggested that the formation of a chemical interaction between MOF-199 and cotton was responsible for the lack of leaching of cooper or MOF after Soxhlet washing with three different solvents. Jin et al. [31] reported the antibacterial activity of MOF-199 synthesized *in situ* over pulp fiber, indicating the existence of an electrostatic attraction between metallic ions and hydroxyl groups of cotton. The composite was remarkably effective against *E. coli* but more effective against *S. aureus*. In 2017, Abdelhameed et al. [32] reported the *in situ* and *ex situ* anchoring of MOF-199 onto cotton fibers, obtaining an *ex situ* Cu content of 4.45%. In 2018, Emam et al. [33] studied the *in situ* synthesis of MOF-199 on PET and nylon and their antimicrobial activity, reporting the formation of a chemical anchoring without any chemical modification of the textile fibers. This same work also mentioned the *ex situ* MOF-199 anchored onto PET and nylon fibers but did not mention the synthetic procedure. In 2020, Emam et al. [34] developed a protective cotton composite through an amalgamation reaction of a cross-linked imidazolate framework (ZIF). The authors incorporated two components based on silicate and zeolitic MOFs, formed directly within the cotton fabrics. When silicate adhered first, besides a significant increase in ZIF amount, the material maintained its color and UV protection even after five consecutive washes. Additionally, textile/MOF composites of Zn, Ti, and other materials have been reported, with UV protection, photocatalytic, and highly hydrophobic properties [29, 30]. On the other hand, the lack of scientific articles on polyester/MOF materials, such as PET, is striking, perhaps because PET is a decidedly inert fiber to processes such as the functionalization necessary to anchor nanoparticles. But considering that within fabrics, PET-cotton (from now on referred to as PETco) fibers are highly commercialized, it is desirable to have PETco materials with antibacterial properties.

Unfortunately, although none of the studies mention it, our experience shows that during the *in situ* synthesis over textiles, more than 75% of the MOF is synthesized in the reaction solution and does not adhere to the fabric, making the scaling up of the process unattractive. Therefore, based on the aforementioned advances and the problems of the *in situ* synthesis, this work describes the immobilization of previously synthesized MOF-199 and MOF UiO-66-NH_2 in carboxylated PETco fibers; or *ex situ* synthesis of textiles/MOF materials. The *ex situ* methodology has substantial advantages over the materials obtained *in situ*. By reacting the already synthesized MOF with a previously functionalized fabric, there is more control over the MOF morphology, homogeneity coverage, and optimization of the MOF amount anchored to the textile. Therefore, and targeting the carbohydrate part of the PETco, radical polymerization was carried out using regenerated activators by electron transfer atom transfer (ATRP-ARGET) to embed in the PETCo the sites where later, *ex situ*, previously synthesized MOF-199

and MOF UiO-66-NH_2 were anchored. Textile materials that showed, in exploratory experiments, activity against *E. coli* and *S. aureus* and moderate leaching stability after various Soxhlet processes in methanol and water.

Experimental

Materials

Zirconium chloride, *L*-ascorbic acid, copper (II) bromide, *N,N*-dimethyl aminopyridine (DMAP), acetone, acetonitrile (ACN), copper (II) nitrate trihydrate, 2-aminoterephthalic acid (H_2BDC-NH_2), ethanol, and methanol were purchased from Merck® (Darmstadt, Germany). 1,3,5-Benzenetricarboxylic acid (H_3BTC), copper (II) acetate hexahydrate, zinc nitrate hexahydrate, triethylamine (TEA), sodium hydroxide, and *N,N*-dimethylformamide were purchased from Panreac-AppliChem GmbH (Darmstadt, Germany). Reference textile of 50/50 polyester/cotton fabric (106 g/m^2) was obtained from Testfabrics Inc. (Pennsylvania, USA). Methacrylic acid, 2-bromoisobutyryl bromide, and *N,N,N′,N″,N″*-pentamethyl diethylenetriamine (PMDETA), were obtained from Sigma-Aldrich Chemie® GmbH. (Steinheim, Germany). 2-Bromoisobutiryl bromide (BIBB) was obtained from Alpha aesar® (Heysham, UK). Reference strains of *E. coli* (ATCC 11775), *S. aureus* (ATCC 6538), agar, and nutrient broth were obtained from HiMedia (India).

Instrumentation

The functionalized fibers were characterized by X-ray diffraction using a Philips Analytical® PW3050/60 diffractometer with Cu anode (Kα: 1.54056 Å), operated at 45 kV voltage and 40 mA acceleration current. The X-ray patterns were analyzed with XPERT-PRO MRD PANalitycal processing software. FTIR-ATR spectra were recorded with a Shimadzu® FTIR solutions spectrophotometer with an ATR module (attenuated total reflectance) with germanium crystal (4000–600 cm^{-1}). SEM micrographs were recorded using a Jeol-JSM-6490 probe for EDX analysis, operated at an acceleration 20 kV beam voltage, and using a Jeol-JSM-6490 probe with a 20 kV beam and a magnification power of 3000x. XPS spectra were measured with an X-ray photoelectronic spectrometer X (NAP-XPS) Specs® with a PHOIBOS 150 1D-DLD analyzer, using an Al-Kα monochromatic (1486.7 eV, 13 kV, 100 W) source with passing energy of 90 eV. High-resolution spectra were recorded using an analysis area of 300 µm × 700 µm and a 20 eV pass. Data were acquired with 0.5 eV steps. All the binding energies were calibrated with the C_{1s} binding energy fixed at 284.6 eV as an internal reference. The UV–visible analyses were performed using a Thermo Evolution-3000 with a double beam and xenon lamp.

MOFs synthesis

MOF-199

The synthesis of free MOF-199 is based on Tranchemontagne et al. [35] and Thi et al. [36] (Scheme S1a). In a regular experiment, separate solutions of 695 mg (3.30 mmol) of H_3BTC and 1198.27 mg (4.95 mmol) of $Cu(NO_3)_2{\cdot}3H_2O$ were prepared in 45 mL of a mixture (1:1:1) of H_2O:EtOH:DMF. This mixture of solvents is important since it solubilizes all the reaction components and works as a high boiling point medium, which allows the synthesis to be carried out under solvothermal conditions. The solutions were mixed in a scintillation vial and closed with rubber stoppers with aluminum caps. The vial was put into an oven at 85 °C for 24 h, to yield bright, tiny, and deep blue crystals (yield 77.78%). These crystals were washed with DMF and acetone, filtered, and dried in vacuum at 80 °C. FTIR-ATR: ν, cm^{-1} = 1639 (s, -C = O); 1443 (b, O-C = O); 1371 (s, = C-O); 1114 (s, O-C = O);759 (s, Cu–O). PXRD (° *2θ*) = 5.75 (200); 9.57 (220); 11.68 (222); 13.56 (400); 15.12 (420); 17.56 (422).

MOF UiO-66-NH_2

MOF was obtained following the procedure of Bunge et al. [37] and Katz et al. [38] (Scheme S1b). 134 mg (0,75 mmol) of H_2BDCNH_2 and 125 mg (0,54 mmol) of $ZrCl_4$ were dissolved separately in 20 mL of DMF. The solutions were sonicated for 20 min, mixed in a scintillation vial, closed with rubber stoppers with aluminum caps, and put into an oven at 120 °C for 24 h. The obtained MOF (yield 71.95%), a fine and clear yellow powder, was washed four times with 10 mL of DMF, filtered, and aired dried for further characterization. FTIR-ATR: ν, cm^{-1} = 3862 (s, N–H); 1651 (s, -C = O), 1562 (b, O-C = O); 1384 (b, N–H); 762 (s, p C–C). PXRD (° 2θ) = 7.60 (111); 8.92 (002); 12.34 (004); 22.44 (115); 25.95 (006).

Textile functionalization

PETco esterification

Insertion of the initiator of polymerization to get PETco-BIBB As mentioned, PETco fibers were modified by ATRP-ARGET surface-initiated (Scheme 1). 1 g of PETco pieces of 4 cm^2 were deposited in a 100 mL round-bottomed flask with 70 mg (3.27×10^{-4} mmol) of DMAP. Then 10 mL (71.14 mmol) of dry TEA were poured with a pipette. After some stirring, 20 mL of dry DMF were added to the flask

Scheme 1 Synthetic pathway for the ATRP-ARGET carboxylation of the cotton fraction in PETco fibers

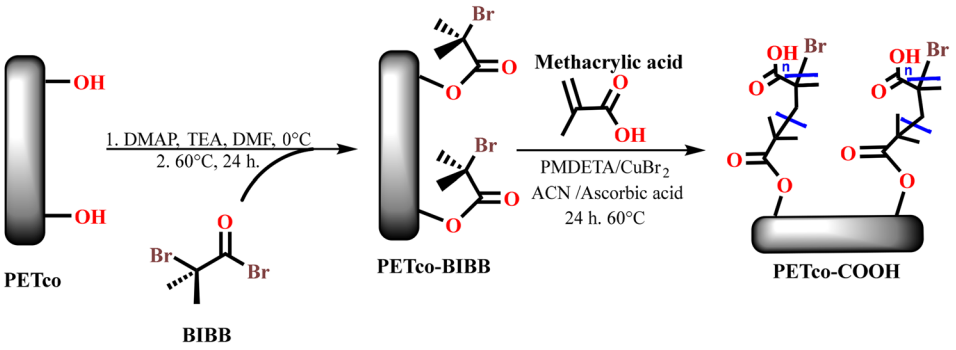

and stoppered with a neoprene cap. Nitrogen was injected to purge the flask while immersed in an ice bath at 0 °C. Ultimately, 3 mL (24.27 mmol) of BIBB were cannulated into the mixture under constant stirring. The low temperature was maintained until the vapors disappeared. Afterward, the temperature was increased to 60 °C for 24 h, and the functionalized textiles were washed thoroughly with water and isopropanol until no bromine was visible. FTIR-ATR: ν, cm^{-1} = 3330 (s, -OH); 2920 (s, -C-H aliphatic); 1720 (s, C = O ester); 1403 (f, $-CH_2$); 1242–1102 (s, = C-O y -C-O); 721 (f, C = C para).

ATRP-ARGET polymerization to get PETco-COOH 1 g of PETco-BIBB was deposited in a 20 mL vial alongside 1 mg (4.47×10^{-3} mmol) of $CuBr_2$, 100 mg (0.58 mmol) of PMDETA, 500 mg (5.80 mmol) of methacrylic acid (MAA), and 1 mL of acetonitrile. After purging the vial with nitrogen, 100 mg (0.57 mmol) of ascorbic acid was added to begin the polymerization. The reaction was kept at 60 °C for 24 h, and the modified textile, PETco-COOH, was washed with water and ethanol and dried at 50 °C in a vacuum oven for further characterization. (Scheme 1). FTIR-ATR: ν, cm^{-1} = 3860 (s, -OH acid); 3330 (s, N–H of amine and -OH of alcohol); 2920 (s, -C-H aliphatic); 1720 (s, C = O amide, acid); 1645 (s, C = O ester); 1502–1342 (f, $-CH_2$ and $-CH_3$); 1246, 1123 (s, C–C and C-O ether); 837 (s, C–Br BIBB); 723 (f, C = C, para substitution). PXRD (° 2θ) = 15.01; 16.6; 22.8; 25.3; 34.6.

Determination of carboxylate content by coulometric titration

Several authors have reported conductimetric methodologies based on indirect titration of -COOH groups to determine the concentration of the carboxylate groups on a fiber. Unfortunately, this technique can be affected by stirring, temperature, viscosity, and other parameters [39–43]. Instead, coulometric methods provide precise and sensible measurements of changes in the concentration of conductive ions (Scheme 2). Then, a precisely measured amount of carboxylated fiber was introduced in a glass reactor, alongside 20 mL of a 0.1 M KCl as the electrolyte, using a Pt electrode (cathode), an Ag electrode (anode), and the pH sensor as the indicator electrode in the acid–base titration. The electrodes were connected in series through a multimeter, and a constant current of 9.97 mA was applied.

Scheme 2 Coulometric titration of the -COOH groups in the textile fibers

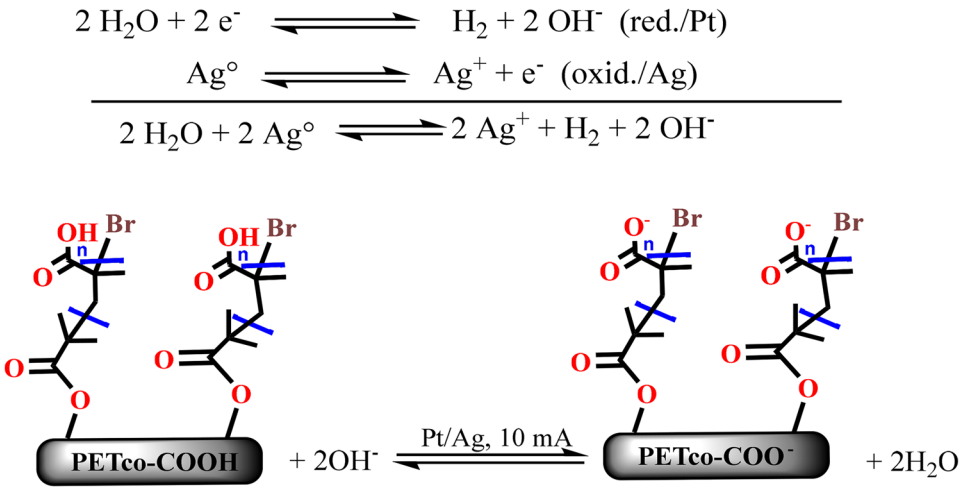

Anchoring of MOF-199 and MOF-UiO-66-NH_2 onto the functionalized textile fibers PETco-COOH

The *ex situ* anchoring of free synthesized MOF-199 and MOF UiO-66-NH_2 was performed following Fu et al. [44] and Zhang et al. [45]. For MOF-199 anchoring, carefully weighed dry PETco-COOH was treated with 0.1 M NaOH to produce ionized carboxylate groups and then reacted with a 0.5 M solution of $Zn(NO_3)_2{\cdot}6H_2O$ to have the PETco-COO-Zn fabric. This treatment is carried out to create cationic exchange places that, in turn, can produce a cationic exchange with the Cu^{2+} cations of the MOF, making easier the anchoring of the nanomaterial. For this, PETco-COO-Zn was placed in a vial alongside a carefully measured amount of previously synthesized MOF-199. Then, 10 mL of acetone were poured with gentle stirring at room temperature to make a suspension of the microparticles. This suspension was then left in the open air until solvent evaporation (12–14 h). The resulting MOF-199@PETco material was dried, weighed, and then washed in a Soxhlet apparatus with water and methanol for 48–72 h. On the other hand, for MOF UiO-66-NH_2@PETco, the procedure was essentially identical, with the only difference that PETco-COOH does not require prior zinc cationization before the *ex situ* synthesis (Scheme 3).

Antibacterial assays

Inhibition assays in Petri dishes

28 g/L of nutrient agar solution was brought to 90 °C in a Schott flask for sterilization and then placed in two previously sterilized Petri dishes. Initial inoculum of both strains, *E. coli* or *S. aureus*, was prepared as follows: 1 µL of the bacteria, suspended in 10 mL of DMSO and 10% glucose, was brought to 10 mL of culture broth with a previously flame-sterilized Pasteur pipette and incubated at 37 °C until reaching the stationary phase. (12 h). Afterward, its turbidity was adjusted using a previously prepared sterile 0.8% NaCl solution until reaching an OD_{625} value of 1–3 × 10^8 CFU/mL. Then, water-soaked pieces (0.5 cm × 0.5 cm) of MOF-199@PETco, MOF UiO-66-NH_2@PETco, pure PETco fiber as a negative control, and PETco in DMSO as a positive control (DMSO at high concentrations has been shown to have strong antimicrobial activity) [36, 37] were placed over the agar plate.

Inhibition assays in liquid culture

Pieces of 0.5 cm × 0.5 cm of MOF-199@PETco, MOF UiO-66-NH_2@PETco, and pure PETco as negative control were sterilized in glass tubes with a lid. On the other hand, 200 mL of 8.5 g/L nutrient broth were prepared and brought to 90 °C for sterilization. After sterilization, the broth was divided into 100 mL Schott flasks, one for each bacterial strain. In each flask, 3.5 mL of the initial inoculum of each bacteria was inoculated, and the flasks were closed and brought to 37 °C for one night until the stationary growth phase. After this time, the OD_{625} of 10 mL liquid culture was determined. Finally, a previously sterilized piece of textile/MOF was added to each tube, measuring the OD_{625} every 1, 3, 5, 9, 19, 24, and 48 h.

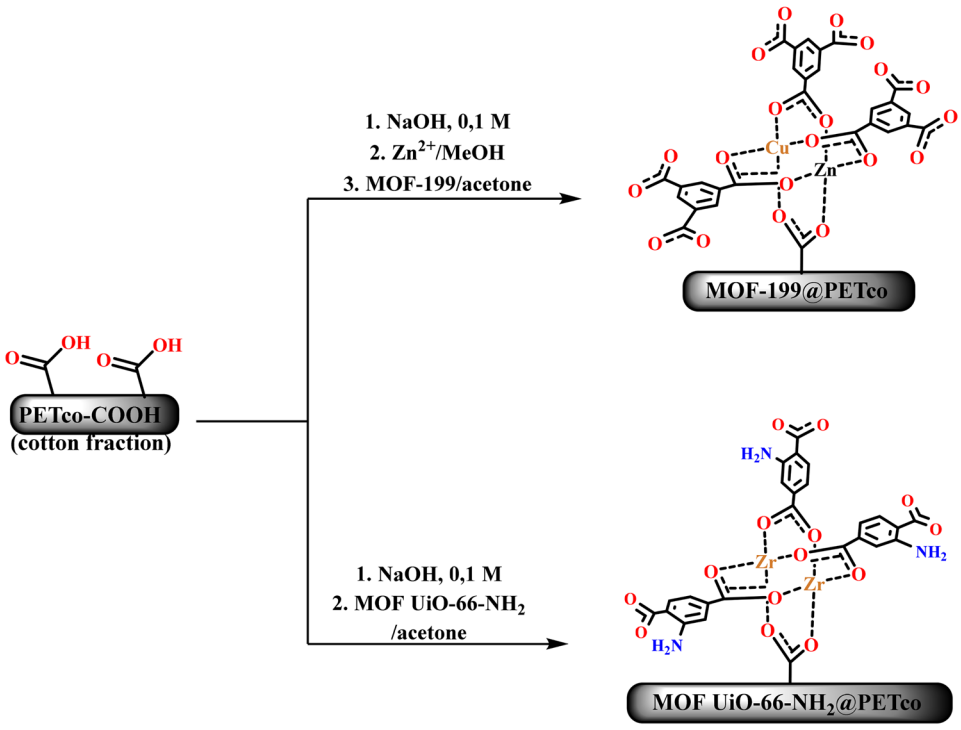

Scheme 3 Synthetic *ex situ* pathway for the chemical immobilization of MOF-199 and MOF UiO-66-NH_2 onto textile fibers to obtain MOF-199@PETco and MOF UiO-66-NH_2@PETco

Results and discussion

Synthesis and characterization of MOFs

MOF-199

After completing the synthesis, the MOF appeared as large, bright bluish crystals that turned darker when heated because of the water loss. The FTIR-ATR spectrum of MOF-199 (Fig. S1a) agrees with the previously reported analysis [31, 38, 46]. Presenting a C = O band at 1639 cm^{-1} from the linker shifted to lower wavenumbers due to the coordination within the network. The bands between 1443 cm^{-1} and 1382 cm^{-1} correspond to = C-H bonds in the aromatic ring of the linker. And the 1273 cm^{-1} band represents the C-O stretching from the carboxylic acids of the free linker, which after forming the MOF, it moves to higher wavenumbers. On the other hand, the PXRD pattern of MOFs (Fig. S1b) presents the expected diffraction peaks for this solid, particularly at low diffraction angles (7, 9.5, 12, 13.7° 2θ), which are in good agreement with the reported by Vellingiri et al. [47] and Thi et al. [36, 48].

MOF UiO-66-NH_2

MOF UiO-66-NH_2 was obtained as a deep yellow powder, showing the FTIR-ATR (Fig. S2a) typical bands reported by Kandiah et al. [49] and Cao et al. [50]. Over 3862 cm^{-1} are appreciated the N–H symmetric and asymmetric stretching bands for the 2-aminoterephthalic acid. At 1651 and 1562 cm^{-1}, C = O and O-C = O signals appear, corresponding to carboxylate groups coordinated to a metal ion. In 1384 cm^{-1} appears, the N–H symmetric flections for the ammine group in the linker structure, and over 655 cm^{-1}, the Zr-O stretching is observed. Additionally, the PXRD patterns (Fig. S2b) show that the obtained product is crystalline and agrees with the previously reported spectra [47]. Between 5–20° 2θ values, the characteristic peaks of MOF UiO-66-NH_2 structure can be observed. These peaks agree with an inner $Zr_6O_4(OH)_4$ core in which a Zr6 octahedron forms triangular phases, alternatively capped by -O (forming a μ_3 bride) or by -OH groups [49].

Characterization of carboxylated PETco textiles

The cotton fraction on PETco was the one carboxylated since it is well known that the PET structure in textiles is highly inert to chemical transformations. In our ATRP-ARGET functionalization, the MAA monomer was used to graft carboxylic groups to the fiber in the presence of a polymerization initiator [51]. It was found that the best relationship MAA/$CuBr_2$/PMDETA/ascorbic was 100/1/2/1, and 1 mL of solvent. This very low amount of solvent was needed to control the polymerization and reduce the possibility of chain terminations. A factor that allowed to carry out the reaction in small vials with just one textile fiber (50–60 mg) at a time. Interestingly, the FTIR-ATR spectra (Fig. 1) show two bands that suggest that the transformation from PETco to PETco-COOH was successful. A new band on 1641 cm^{-1} in PETco-COOH (Fig. 1, black) due to the presence of a new type of -C = O group in the structure. And the most evident

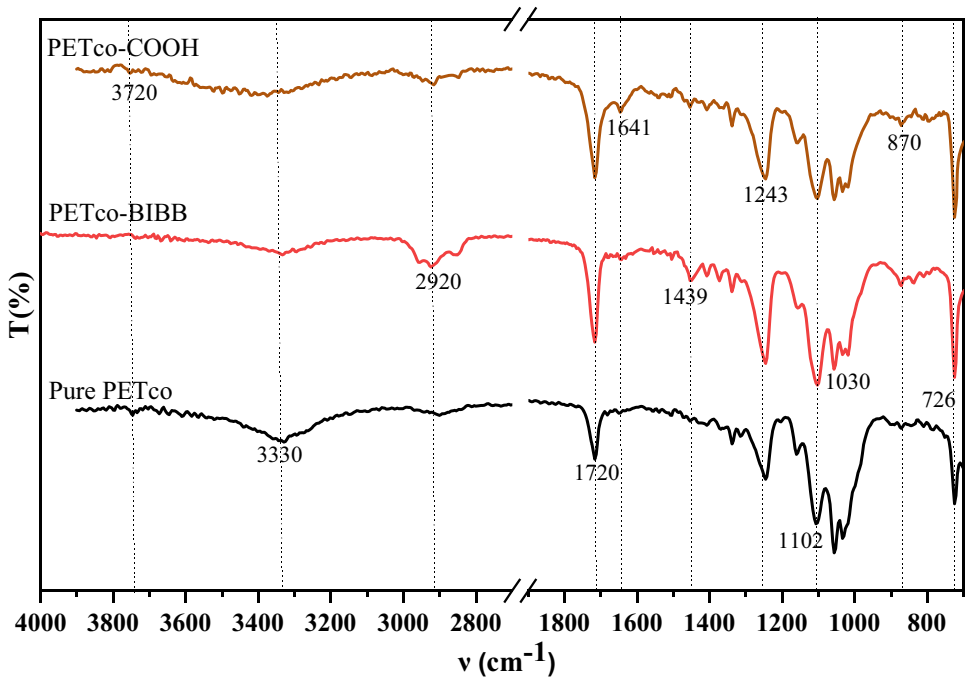

Fig. 1 FTIR-ATR spectra of pure PETco (black), PETco-BIBB (red), and PETco-COOH (brown)

Table 1 Concentration of carboxylic groups for PETco and PETco-COOH

Textile fiber	[COOH] mmol/g
PETco	0.00
PETco-COOH	0.030

appearance of stretch absorption bands over 2920 cm^{-1} due to the grafting with MAA that increases the C-H sp^3 groups.

The amount of carboxylic (-COOH) groups on PETco-COOH was determined by coulometric titration to corroborate further the results obtained by FTIR-ATR, using the R software and Eq. (1). Where $t_{end\ point}$ is the time (in seconds) at the endpoint of the titration curve, i is the constant current (in Amperes), and the conversion factors required for the equation are depicted. The results show that, although the obtained concentration is relatively low, these are in good agreement with the expected and reported in the literature (Table 1) [52, 53].

$$\frac{mmol\ COOH}{g\ textile} = t_{end\ point} \cdot i(A) \cdot \frac{1\ mol\ e-}{96485{,}33\ C} \cdot \frac{1\ mol\ H^+}{1\ mol\ e-} \cdot \frac{1\ mol\ COOH}{1\ mol\ H^+} \cdot \frac{1\ 000\ mmol}{1\ mol} \cdot \frac{1}{g\ textile} \quad (1)$$

The low concentration of carboxyl groups obtained in PETco-COOH could be because a very low proportion of the cotton in the PETco fibers is superficially exposed, making the functionalization through the ATRP-ARGET polymerization described more complex. The presence of the PET fraction may be responsible for inhibiting the polymerization since it could hide the active -OH sites in cotton. It is important to point out that there are no reports of ATRP-ARGET carboxylation reactions onto PETco fibers to the best of our knowledge. On the other hand, the XRD of PETco and PETco-COOH did not show differences in the position of the diffraction peaks before and after the chemical transformation (Fig. 2), which suggests that the crystalline phase of the cotton fraction in PETco did not undergo changes despite the chemical transformation carried out.

Characterization of ex situ synthesized MOF@PETco

MOF-199@PETco

The FTIR-ATR spectra (Fig. 3a) show a clear superposition of the bands for the free MOF and the MOF grafted fiber. In particular, the bands around 1646 and 1543 cm^{-1} in MOF-199 (Fig. 3a, blue) and MOF-199@PETco (Fig. 3a, red) correspond to the stretching of C = O in the BTC linker coordinated to the metal center. Additionally, the XRD pattern of MOF-199@PETco can be constructed as a superposition of the diffraction peaks of PETco-COOH and MOF-199 (Fig. 3b). Where the textile/MOF show signals at low 2θ angles (5.75, 9.57, 11.68, 13.56° 2θ) belonging to the MOF-199, which is not overshadowed by the broad diffraction peaks corresponding to the PETco-COOH fiber. DRX patterns agree with previous reports on cotton-MOF materials [23, 47, 54].

On the other hand, the general XPS spectra of MOF-199@PETco (Fig. S5a in supporting information) were used to determine the concentration of Cu^{2+} and Zn^{2+} quantitatively, and the results are shown in Table 2. The high-resolution spectra of copper (Cu_{2p}) and oxygen (O_{1s})

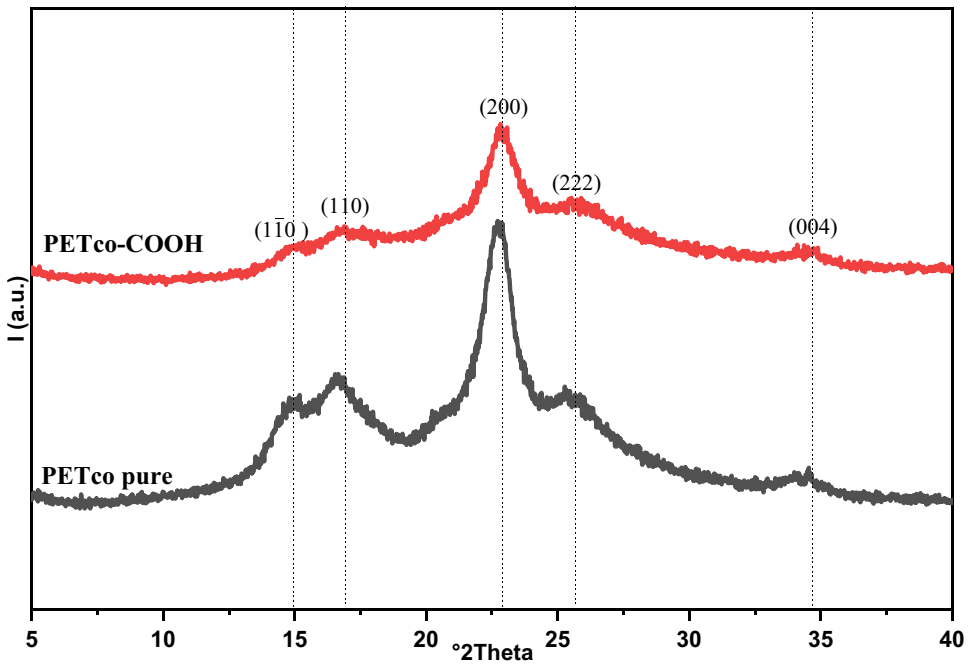

Fig. 2 XRD patterns of: PETco pure (black) and PETco-COOH (red)

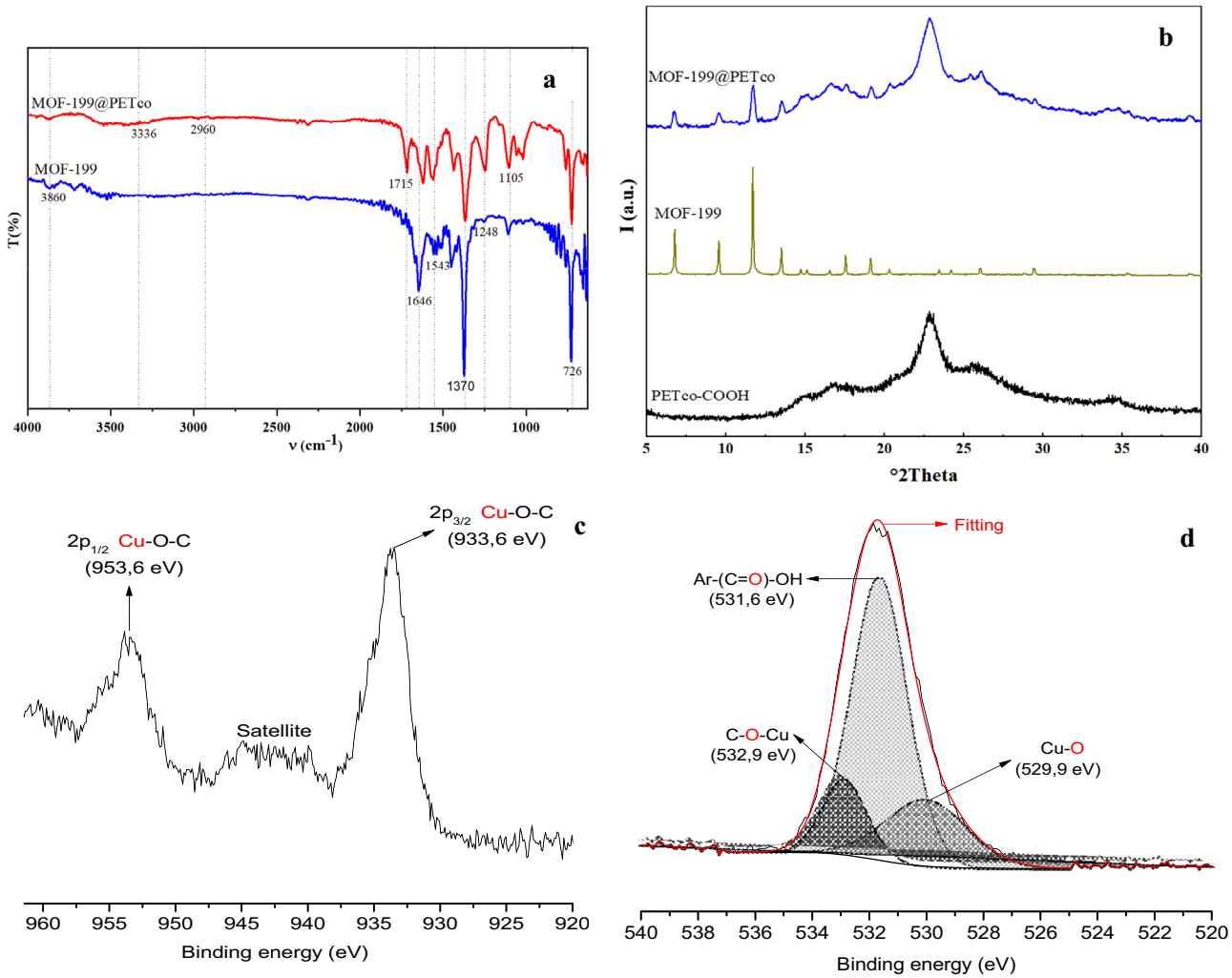

Fig. 3 **a** FTIR-ATR spectra of MOF-199 and MOF-199@PETco; **b** XRD spectra of PETco-COOH, MOF-199 and MOF-199@PETco; **c** XPS high resolution Cu_{2p} spectra, and; **d** O_{1s} spectra in MOF-199@PETco

were used to analyze their chemical interactions (Fig. 3c and d, respectively). In Fig. 3c, the $Cu_{2p(3/2)}$ signal can be observed at a binding energy of 933.6 eV, which along the satellite signals around 943 eV indicate the presence of Cu^{2+}. Additionally, the $Cu_{2p(1/2)}$ signal towards 953.6 eV ($Cu_{2p(3/2)}$–$Cu_{2p(1/2)}$ = 20 eV) also indicate the presence of Cu^{2+} bonded to atomic oxygen [55].

Concerning O_{1S} spectra (Fig. 3d), the deconvolution shows two signals at 532.9 eV and 529.9 eV, which can be associated with atomic oxygen bonded to Cu. Additionally, at 531.6 eV, the higher intensity signal can be related to the oxygen of carbonyl groups. However, due to the amplitude of this signal, it can be analyzed as the carbonyl contribution belonging to the carboxylic acid (not anchored with the MOF) and ester groups. Furthermore, as summarized in Table 2, the surface Cu^{2+} concentration turned out to be 4.47% atomic in the MOF-199@PETco fibers. According to previously obtained results of MOF-199, both *in situ* [27, 47, 50] and *ex situ* [26, 27] attached to textile cotton fibers and PET fibers, a substantial enhancement of the amount of Cu^{2+} has been encountered in this work. This could be explained thanks to the presence of Zn^{2+} ions previously anchored to the carboxylated PETco. The XPS results also report a remaining concentration of Zn^{2+} of 1.70% atomic for MOF-199@PETco, which implies that the concentration of Cu^{2+} on the fiber surface could be increased. XPS spectra also show two signals at 953.6 eV and 955.6 eV, which correspond to the binding energy of $Zn_{2p(1/2)}$ and $Zn_{2p(3/2)}$, respectively (Fig. S3b). These signals correspond

Table 2 Atomic percentages in MOF-199@PETco composite surface

MOF@Fiber	Atomic percentages in surface			
	$C_{(1\,s)}$	$O_{(1\,s)}$	$Cu_{(2p)}$	$Zn_{(2p)}$
MOF-199@PETco	49.25	44.58	4.47	1.70

to the Zn–O bonds, values in agreement with the XPS spectra reported by Fu et al. [44] and Moulder et al. [55]. The XPS spectrum of blank cotton can be observed in Fig. S4, alongside the deconvoluted signals of C_{1s} (Fig. S3a) and O_{1s} (Fig. 3d).

The morphology characterization of obtained materials was carried out by SEM to gather a graphic register of the presence of MOF-199 onto the textile fibers and verify the integrity of the morphological characteristics of the nanocrystals of MOF after the *ex situ* immobilization. SEM micrographs (Fig. 4a and b) show that MOF-199 maintained in some cases the reported octahedral morphology after anchoring, with smooth faces and visible edges. The SEM micrographs shown in Fig. 4a and b for both blend materials clearly indicate that the coating with the solid MOF was not regular, and the particles agglomerated randomly. This is a consequence of using the suspension anchoring methodology on a solid (the textile fiber). Nevertheless, as shown in the antibacterial tests, the inhibition activity was satisfactory and constant for at least 48 h. Still, it is feasible that an improvement in this activity is closely related to the enhancement of the homogeneity of the anchoring and covering. Regarding the integrity of the particle morphology, a comparison between the micrographs showing the morphology of free MOF-199 (Fig. S7a and b) and the MOF/PETco material (Fig. 4a and b) can be made. As observed, the morphology of these MOFs maintains its integrity despite the presence of solvent and constant stirring; however, the

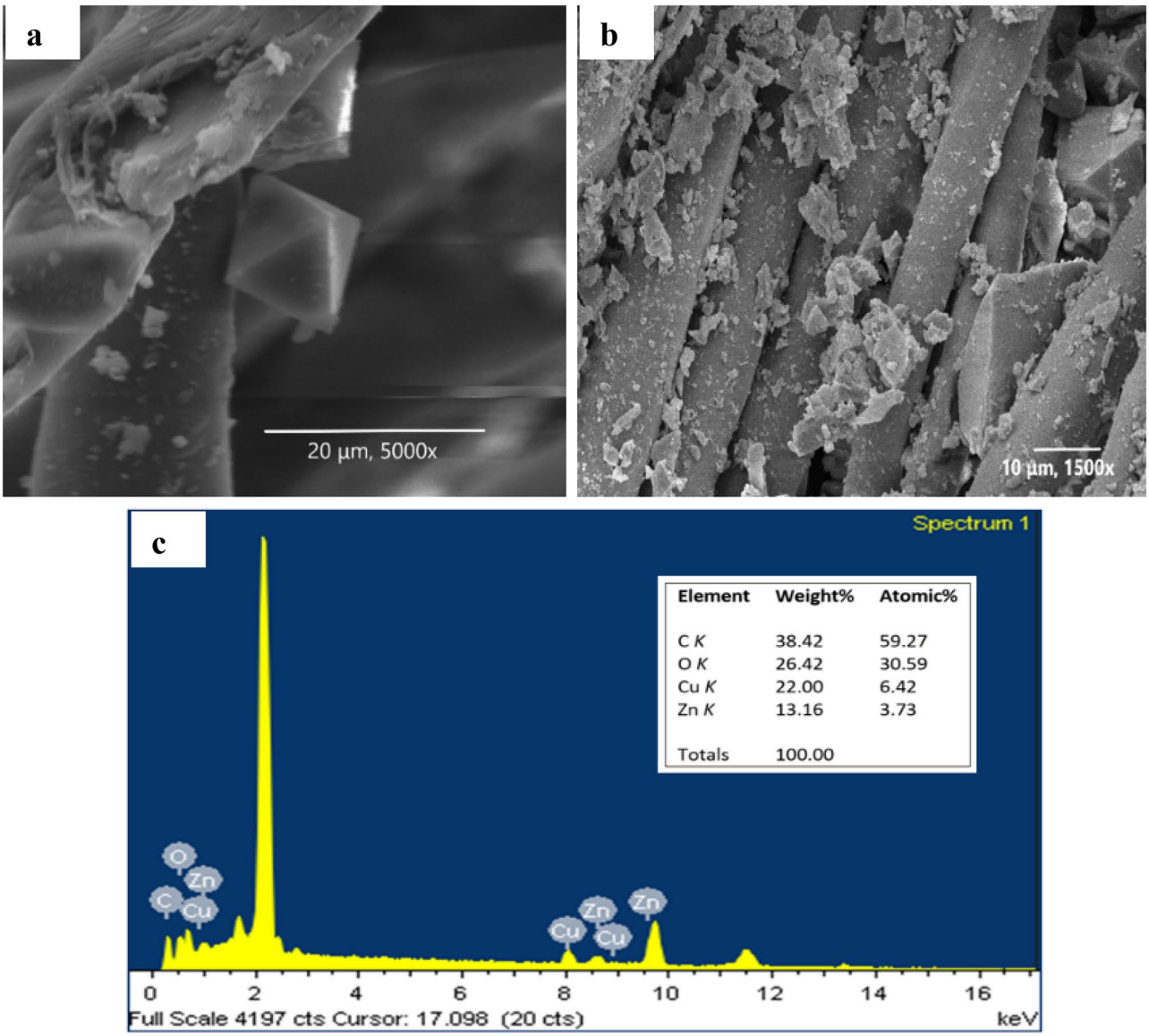

Fig. 4 SEM images of MOF-199@PETco at; **a** 5000× and 20 µm, and **b** 1500× and 10 µm. **c** EDX spectrum of MOF-199@PETco

decrease in the size of random particles can be observed as well. This can be attributed to the strength of the stirring, which predominantly affects larger crystals. Although, this does not affect the antibacterial effects of the nanostructured material.

Complementary EDS analyses were also performed to estimate the concentration of Cu^{2+} and Zn^{2+} on the surface of the textiles. The weight percentage of copper in MOF-199@PETco, 22% wt. (6.42% atomic) agrees with the expected results (Fig. 4c) and the estimated percentages calculated.

MOF UiO-66-NH_2@PETco

Following the immobilization route shown in Scheme 3, the MOF UiO-66-NH_2@PETco textile was obtained. This was mainly due to the chemical character as hard Pearson acid and base of the Zr^{4+} and the carboxylate ligands in the fiber, respectively; in this case, there was no need for the previous ionization of the PETco-COOH fiber with NaOH. Zr^{4+} is a small charge-concentrated cation with low polarizability, and in its highest oxidation state, with a highly energetic LUMO orbital without readily excitable electrons. Meanwhile, the carboxylate anion is a bidentate small, electron-donating ligand with low polarizability and high electronegativity, prone to form chemical bonds with empty orbitals of high energy [56].

The FTIR-ATR spectra of MOF UiO-66-NH_2@PETco (Fig. 5a) show two characteristic vibrations of MOF UiO-66-NH_2, on 1562 cm^{-1} and 1389 cm^{-1}, which are not present in the PETCo-COOH fiber (Fig. 1), indicating that the MOF is part of the MOF/textile system. Additionally, the band appearance at 1718 cm^{-1} corresponding to the stretching in and out of the plane of the O-C = O group in PETco-COOH (Fig. 1) suggests that several -COOH groups in the fiber are free of MOF, as expected. Finally, towards 655 cm^{-1}, the stretching that has been attributed to the Zr-O bond is observed.

The XRD spectra of the textile/MOF material (Fig. 5b) show a good overlapping of the diffraction signals for MOFs and the PETco fiber. The intensity of the diffraction patterns in PETco-COOH (Fig. 5b, pink) is almost unchanged after treatment with the MOF, as seen in the diffraction pattern of MOF UiO-66-NH_2@PETco (Fig. 5b, red). As mentioned before, ATRP-ARGET reaction for PETco exerts no influence on the diffraction pattern of the fibers. As seen in the XRD spectra for PETco (Fig. 2), the peaks corresponding to $(1\bar{1}0)$, (110), (200), and (004) diffraction planes for the cotton fraction and (222) for PET remain with no modifications, maintaining the pristine topology of the hybrid textile/MOF material [45].

For its part, in the high-resolution spectra of Zr_{3d} (Fig. 5c), the two signals at 182.8 eV ($Zr_{3d(5/2)}$) and 185.2 eV ($Zr_{3d(3/2)}$) indicate the presence of Zr^{4+} bonded to oxygen, i.e., the Zr^{4+} ion on the MOF coordinated to the -COO groups of the PETco. This is consistent with that reported by the authors mentioned above and by Moulder et al. [55].

The general XPS spectra for the MOF UiO-66-NH_2@PETco fiber (Fig. S5b) showed the expected signals corresponding to Zr_{3d}, C_{1s}, O_{1s}, and N_{1s}, related to the MOF anchored and also was used to quantify the elements on the surface (Table 3). The atomic percentage of Zr^{4+} is 12.06, higher than the value reported by other works related to the anchoring of MOFs of the UiO family over this type of fiber [52, 53]. Additionally, the signals of the deconvoluted O_{1s} spectra (Fig. 5d) in the MOF UiO-66-NH_2@PETco fiber; C-O-Zr (533.2 eV), -C-(C = O)-OH (531.6 eV), and Zr-O (529 eV) were assigned according to Ardila-Suárez et al. [57], who reports the study by XPS of three Zr MOFs using H_2BDC-NH_2 as a linker. The signals in which Zr is present are of particular importance since by comparing the general XPS spectrum of carboxylated cotton fibers as a reference (Fig. S4) and those for MOF UiO-66-NH_2@PETco (Fig. S5b) allows us to affirm that the anchoring of Zr^{4+} ions did occur indeed. The binding energy of the C-O-Zr and Zr-O bonds remains constant in the MOF UiO-66-NH_2@PETco fiber, concerning the same energy of the MOFs in the pure state reported by Ardila-Suárez et al. [57]. The other analyzed elements (C_{1s} and N_{1s}) are also present, and their deconvoluted signals are shown in Fig. S3c and d.

Finally, the MOF UiO-66-NH_2@PETco composites were also analyzed by SEM. As depicted in Fig. 6a and b, the obtained SEM micrographs show particles of approximately 500 nm to 1 µm with no regular or polyhedral shapes, which is in good agreement with previous reports of this MOF anchored onto cotton textile fibers [36, 52, 53, 58]. As seen in the SEM micrographs of the free UiO-66-NH_2 (Fig. S7c and d), the material preserves its morphological integrity after the anchorage on PETco textile fibers. As the size of the crystals of this MOF is small, it can be observed that a more homogeneous covering onto the textile fiber was achieved, compared with the MOF-199@PETco material. It is a reasonable conclusion that, when reducing the size of the anchored material, its contact surface increases as well as the homogeneity and stability of the anchorage. Furthermore, EDS analysis on MOF UiO-66-NH_2@PETco (Fig. 6c) found 14.63% wt (2.56% atomic) of Zr^{4+}. Percentages higher than previously reported in cotton and other fibers [26, 52].

Inhibition assays

Inhibition assays in Petri dishes

The preliminary bactericidal essays of *ex situ* anchored MOFs/PETco systems showed that the MOF material undergoes lixiviation from the textile fiber, forming inhibition

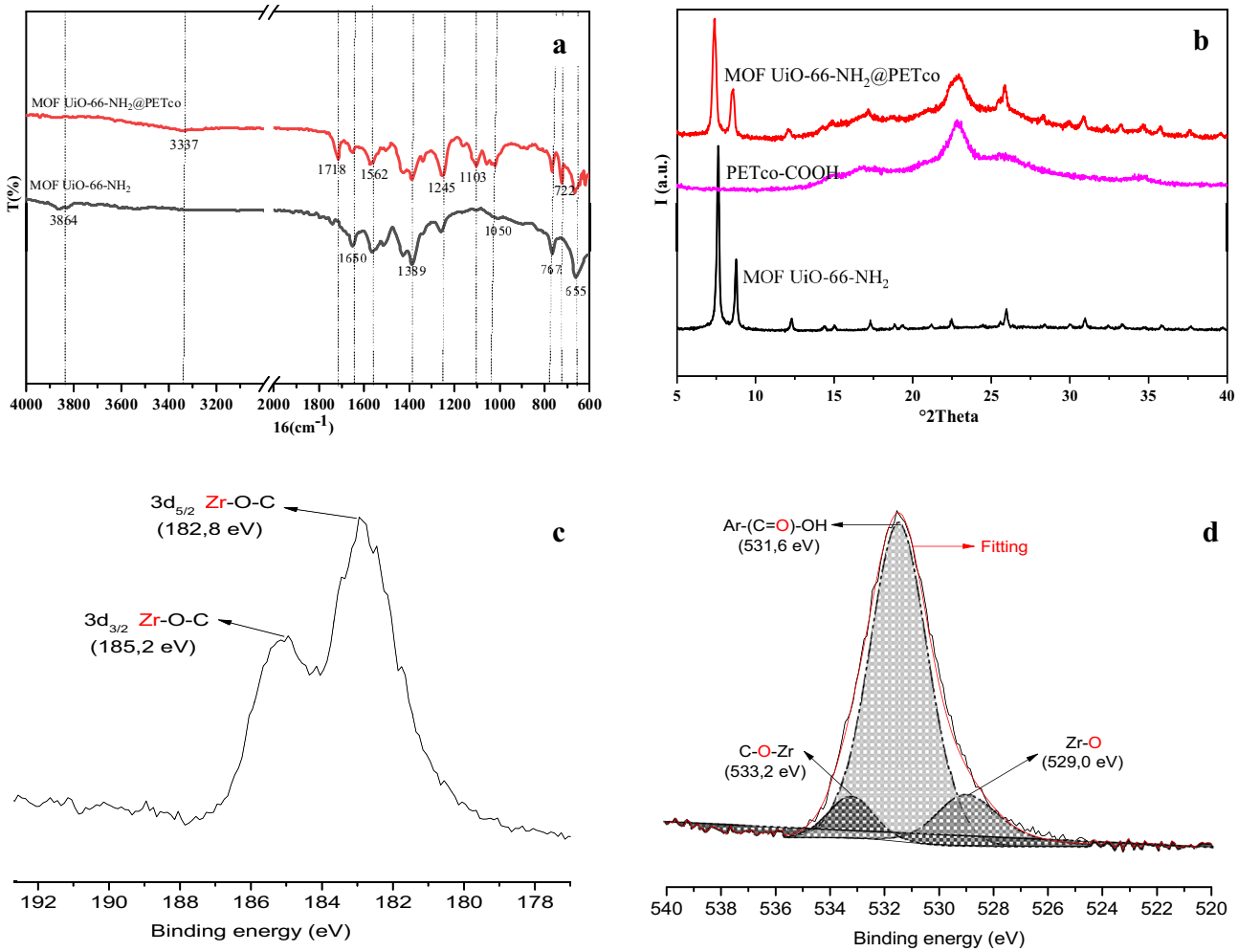

Fig. 5 **a** FTIR-ATR spectra of MOF UiO-66-NH_2 and MOF UiO-66-NH_2@PETco, **b** XRD spectra of PETco-COOH, MOF UiO-66-NH_2, and MOF UiO-66-NH_2@PETco. High-resolution XPS spectra of; **c** Zr_{3d}, and **d** O_{1s} of MOF UiO-66-NH_2@PETco

halos in the nutrient agar. In our preview experiments, carried out with *in situ* attached MOFs/cotton systems, we did not observe this type of lixiviation, indicating a stronger chemical interaction between the metal–organic framework and the textile fiber. Therefore, based on this observation, improvements in the *ex situ* anchoring methodology of the MOFs on the fiber are currently underway. The most evident inhibition halos for the *E. coli* assay were presented by MOF-199@PETco. In this case, the MOF not only inhibited growth in the contact area between MOF-199@PETco and the nutrient gel, but the MOF, or its parts, slowly diffused through the gel, creating inhibition halos. Contrarily, it was observed that bacteria grew easily around MOF UiO-66-NH_2@PETco, and only bacterial growth was inhibited in the contact area between the agar and the fabric. Similarly, in the test with *S. aureus*, it was observed that the inhibition halos are significantly large for MOF-199@PETco than for the MOF UiO-66-NH_2@PETco. Interestingly, and contrary to previously reported, the positive control (pure PETco soaked in DMSO) did not inhibit *E. coli* and *S. aureus* [59].

In general, against the two bacteria studied, the textile inhibitory activity with MOF UiO-66-NH_2 was lower than with MOF-199. Now, if we assume that the growth rate of the bacteria is directly related to the lesser or greater intensity of the color of the coating formed by the culture around the fabric (taking into account also the cotton blanks and positive controls), the MOF UiO-66-NH_2@PETco presented a bacteriostatic effect, while the MOF-199@PETco exhibited an antibacterial effect.

Table 3 Atomic percentages in MOF UiO-66-NH_2@PETco composite surface

MOF@Fiber	Atomic percentages in surface			
	$C_{(1\,s)}$	$O_{(1\,s)}$	$Zr_{(3d)}$	$N_{(1\,s)}$
MOF UiO-66-NH_2@PETco	44.28	41.99	12.06	1.67

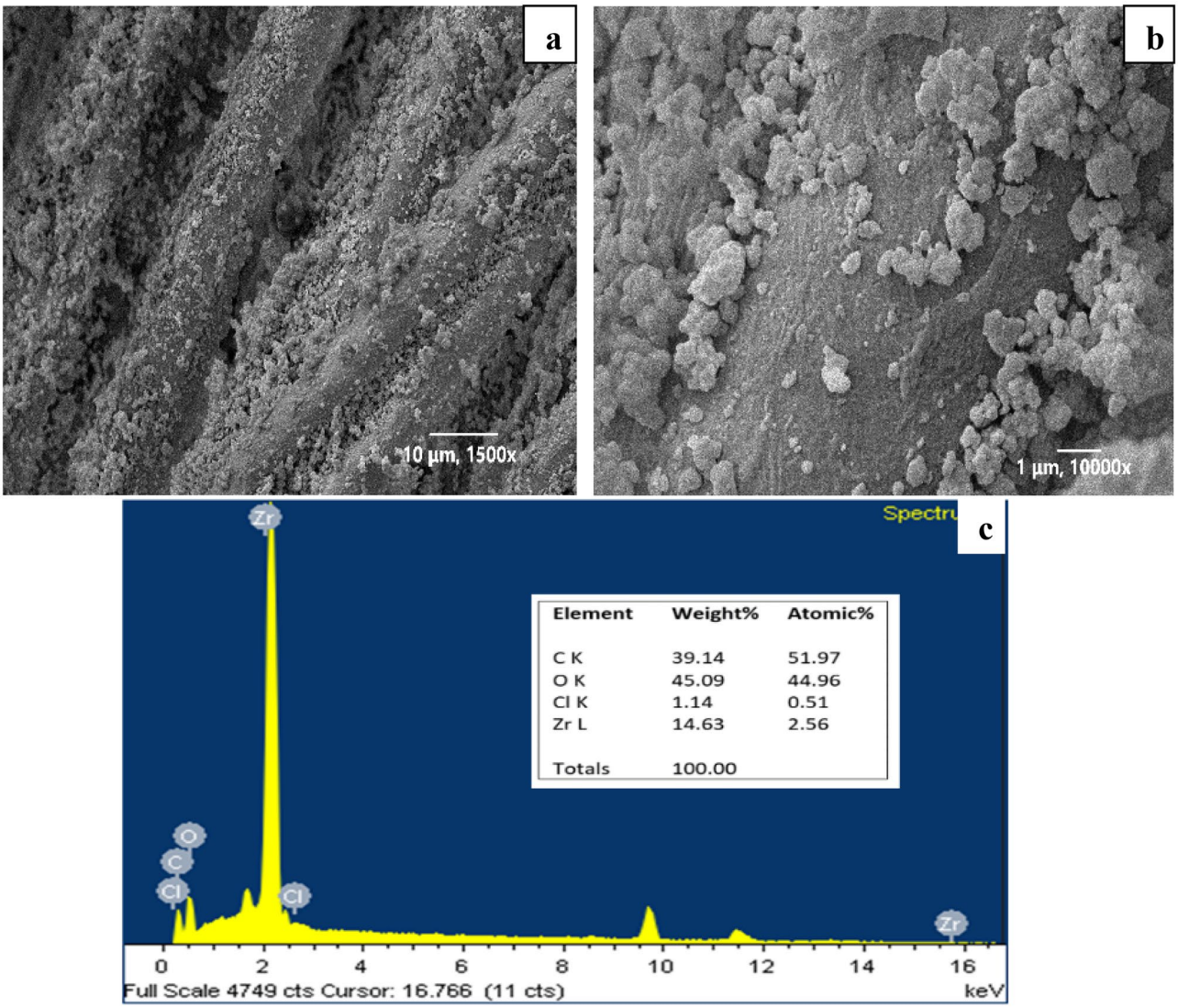

Fig. 6 SEM images of MOF UiO-66-NH_2@PETco at; **a** 1500× and 10 µm, and **b** 10000× and 1 µm. **c** EDX spectrum of MOF UiO-66-NH_2@PETco

Inhibition assays in liquid cultures

Considering the results found with the Petri dishes test, the analysis with liquid cultures could corroborate the previous results and allow better quantifying of the antibacterial or bacteriostatic effect of the textiles. Then, the inhibition curves for *E. coli* (Fig. 7a) show a notorious inhibitory effect by the textil/MOF systems. Starting with an inoculum of approx. 2.02×10^8 bacteria (OD_{625} of 0.161), the PETco blank did not show any inhibition during the 48 h of the experiment but a rapid increase in bacteria after 10 h. On the contrary, MOF-199@PETco and MOF UiO-66-NH_2@PETco systems showed a considerable decrease in bacteria throughout the experiment. It is clear that although by using the textile/MOF systems, there is a significant decrease in the growth rate of *E. coli* to the PETco blank (the number of bacteria decreases at least three times), there is no total inhibition nor total death of bacteria. Although we did not find reports of the antibacterial activity of MOFs synthesized *ex situ* on PETco, there are reports of antibacterial activity of the same MOFs synthesized *in situ* on cotton. Interestingly, in the *in situ* materials reported, the copper amount is less than that found in this work doing the *ex situ* process, but *in situ* materials have higher antibacterial activities. Therefore, it could be thought that the amount of copper in the textile is not directly related to the antibacterial activity. Similarly, for MOFs that contain Zr^{4+} such as those of the UiO MOF family, it has been reported that materials obtained *in situ* are not as good antibacterial as those obtained with MOF-199. In fact, Zr-MOF-based materials are commonly post-functionalized with other

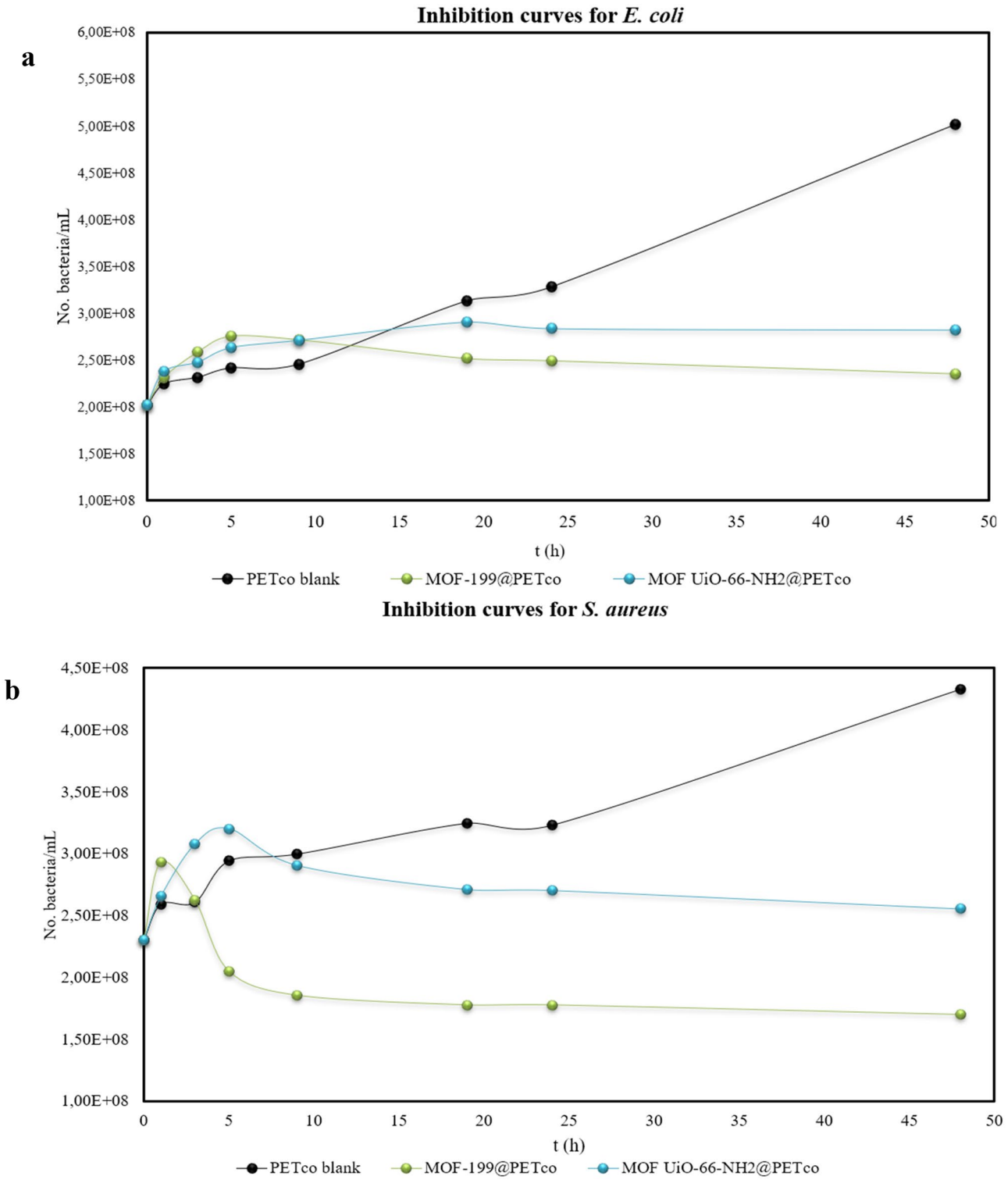

Fig. 7 Inhibition curves of PETco blank (black), MOF-199@PETco (light blue) and MOF UiO-66-NH_2@PETco (green) for; **a** *E. coli* and **b** *S. aureus*

biocidal materials known as Ag nanoparticles (AgNP) or irradiated with ultraviolet light [55, 60–63]. However, the factors that relate to the strength of the anchor between textile fibers and MOF, and the size of the MOF crystals, among others, cannot be ruled out as possible influencers on the intensity of antibacterial activity. Factors under study by our group currently.

On the other hand, the textile/MOF systems presented a much more effective and significant inhibition for *S. aureus* (Fig. 7b). Like that given for *E. coli*, the PETco blank shows constant growth throughout the experiment. Behavior that contrasts strongly with the significant inhibition carried out by the MOF-199@PETco material, reducing the number of bacteria by almost half before 48 h, which confirms the strong inhibitory power of Cu. For its part, although MOF UiO-66-NH_2@PETco follows a similar behavior to that of MOF-199@PETco described above, its inhibitory power is much lower in the experiment time interval. If the number of bacteria at 0 h is compared with those at 48 h, they are not equal to or less than the initial number. This would allow us to conclude that MOF UiO-66-NH_2@PETco textile is not an inhibitor of bacterial growth, but it can slow down its growth and maintain a high population control [64, 65]. Significantly, as stated previously, the intensity of the color of the coating of the Petri dishes cultures can be related to the concentration of bacteria. The liquid culture assays corroborate these observations. Figure 7a and b show that the inhibition was more substantial and pronounced in *S. aureus* than in *E. coli* and Fig. S6 in supplementary information shows that the inhibition activity in terms of percentage was notoriously higher with MOF-199@PETco material (20.31% for *E. coli* and 49.79% for *S. aureus*) than with MOF UiO-66-NH2@PETco material at the end of the 48 h of analysis. In the Petri dish assays, the inhibition of *S. aureus* caused the total disappearance of the bacterial coating on the surroundings of the PETco textile fibers with MOFs (specially MOF-199). It is important to clarify that, since our principal aim was the development of the textile/MOF blend via *ex situ* synthesis, durability essays of the antibacterial activity were not performed in this work. The performed antibacterial essays are partially based upon previous research projects in our group, which utilized ASTM regulations to design the experiments to test the antibacterial power of textile fibers. For all of the above, we are working to achieve in the near future that the functionalized textiles obtained can be tested under in vivo conditions with patients with nosocomial infections []. Since in addition to the antibacterial power, the textile/MOF showed that it could be used continuously for 48 h without loss of antibacterial power, with an exponential increase in biocidal power according to the inhibition curves in Fig. 7a and b.

Conclusions

The ATRP-ARGET carboxylation of the cellulosic part in a low reactivity textile fiber such as PET-cotton allowed free synthesized MOF to be anchored. This makes the synthesis of MOF-199@PETco and MOF UiO-66-NH_2@PETco materials possible through an *ex situ* methodology. These textile/MOF systems showed good stability under Soxhlet wash conditions, suggesting that, like *in situ*, *ex situ* synthesis allows the formation of chemical interactions between MOF and textile. FTIR-ATR, XRD, and XPS analysis confirmed this, among others, by demonstrating the presence of MOF in the fabric and showing interactions between the metal of the MOF and the textile. And although the antibacterial activity against *E. coli* and *S. aureus* was lower than that reported by similar *in situ* textile/MOF systems (the reasons for these differences are currently being studied), the results showed that the *ex situ* synthesis of MOF on textiles could make the industrial scale-up of MOF-based antibacterial textiles production attractive.

Supplementary Information The online version contains supplementary material available at https://doi.org/10.1007/s10965-022-03216-x.

Funding Open Access funding provided by Colombia Consortium. We acknowledge to Universidad Nacional de Colombia, to "Jóvenes Investigadores e Innovadores" Fellowship of Ministerio de Ciencia, Tecnología e Innovación of Colombia (Grant 812–2018) and to Universidad de Antioquia for XPS and SEM/EDS analysis of the obtained materials.

Declarations

Conflict of interest The manuscript was prepared and revised with the participation of all the authors, who declared that no conflict of interest could damage the validity of the results presented.

References

1. Hoskins B, Robson R (1989) Infinite Polymeric Frameworks Consisting of Three Dimensionally Linked Rod-Liked Segments. J Am Chem Soc 111:5964–5965. https://doi.org/10.1021/ja00197a079
2. Hoskins BF, Robson R (1990) Design and Construction of a New Class of Scaffolding-like Materials Comprising Infinite Polymeric Frameworks of 3D-Linked Molecular Rods. A Reappraisal of the Zn(CN)2 and Cd(CN)2 Structures and Synthesis and Structure of the Diamond-Related Frameworks. J Am Chem Soc 112:1546–1554. https://doi.org/10.1021/ja00160a038
3. Yaghi OM, O'Keeffe M, Ockwig NW et al (2003) Reticular synthesis and the design of new materials. Nature 423:705–714. https://doi.org/10.1038/nature01650

4. Rosi NL, Kim J, Eddaoudi M et al (2005) Rod Packings and Metal - Organic Frameworks Constructed from Rod-Shaped Secondary Building Units. J Am Chem Soc 127:1504–1518
5. Tranchemontagne DJ, Mendoza-Cortés JL, O'Keeffe M, Yaghi OM (2009) Secondary building units, nets and bonding in the chemistry of metal-organic frameworks. Chem Soc Rev 38:1257–1283. https://doi.org/10.1039/b817735j
6. Choi JY, Huang R, Uribe-romo FJ et al (2006) Exceptional chemical and thermal stability of zeolitic imidazolate frameworks. Proc Natl Acad Sci 103:10186–10191. https://doi.org/10.1073/pnas.0602439103
7. Assen AH, Yassine O, Shekhah O et al (2017) MOFs for the Sensitive Detection of Ammonia: Deployment of fcu-MOF Thin-Films as Effective Chemical Capacitive Sensors. ACS Sens 2:1294–1301. https://doi.org/10.1021/acssensors.7b00304
8. Ozer RR, Hinestroza JP (2015) One-step growth of isoreticular luminescent metal–organic frameworks on cotton fibers. RSC Adv 5:15198–15204. https://doi.org/10.1039/C4RA15161E
9. Wu MX, Yang YW (2017) Metal-Organic Framework (MOF)-Based Drug/Cargo Delivery and Cancer Therapy. Adv Mater 29:1–20. https://doi.org/10.1002/adma.201606134
10. Smith MK, Mirica KA (2017) Self-Organized Frameworks on Textiles (SOFT): Conductive Fabrics for Simultaneous Sensing, Capture, and Filtration of Gases. J Am Chem Soc 139:16759–16767. https://doi.org/10.1021/jacs.7b08840
11. Abdelhameed RM, Simões MMQ, Silva AMS, Rocha J (2015) Enhanced Photocatalytic Activity of MIL-125 by Post-Synthetic Modification with CrIII and Ag Nanoparticles. Chem Eur J 21:11072–11081. https://doi.org/10.1002/chem.201500808
12. Casey AL, Adams D, Karpanen TJ et al (2010) Role of copper in reducing hospital environment contamination. J Hosp Infect 74:72–77. https://doi.org/10.1016/j.jhin.2009.08.018
13. Neufeld BH, Neufeld MJ, Lutzke A et al (2017) Metal-Organic Framework Material Inhibits Biofilm Formation of Pseudomonas aeruginosa. Adv Funct Mater 27:1702255. https://doi.org/10.1002/adfm.201702255
14. Czaja AU, Trukhan N, Müller U (2009) Industrial applications of metal–organic frameworks. Chem Soc Rev 38:1284. https://doi.org/10.1039/b804680h
15. Pramudya Y, Mendoza-Cortes JL (2016) Design Principles for High H2 Storage Using Chelation of Abundant Transition Metals in Covalent Organic Frameworks for 0–700 bar at 298 K. J Am Chem Soc 138:15204–15213. https://doi.org/10.1021/jacs.6b08803
16. Eliseeva SV, Bunzli J-CG (2010) Lanthanide luminescence for functional materials and bio-sciences. Chem Soc Rev 39:189–227. https://doi.org/10.1039/B905604C
17. Smaldone RA, Forgan RS, Furukawa H et al (2010) Metalorganic frameworks from edible natural products. Angew Chemie Int Ed 49:8630–8634. https://doi.org/10.1002/anie.201002343
18. Mueller U, Schubert M, Teich F et al (2006) Metal-organic frameworks - Prospective industrial applications. J Mater Chem 16:626–636. https://doi.org/10.1039/b511962f
19. Morris RE (2013) Anti-microbial metal organic framework. Patent EP2603076 A, 2
20. Lu X, Ye J, Zhang D et al (2014) Silver carboxylate metal – organic frameworks with highly antibacterial activity and biocompatibility. J Inorg Biochem 138:114–121. https://doi.org/10.1016/j.jinorgbio.2014.05.005
21. Tamames-Tabar C, Imbuluzqueta E, Guillou N et al (2015) A Zn azelate MOF: Combining antibacterial effect. Cryst Eng Comm 17:456–462. https://doi.org/10.1039/c4ce00885e
22. Ibrahim N, Basma E, Sharaf S (2019) Functional Finishes for Cotton-Based Textiles: Current Situation and Future Trends. In: Shabbir M (ed) Textile and Clothing- Environmental Concerns and Solutions. Wiley-Scrivener, USA, pp 131–190
23. Ibrahim N, Basma E, Abdellatif F (2018) Advanced Materials and Technologies for Antimicrobial Finishing of Cellulosic Textiles. In: Yusuf M (ed) Handbook of Renewable Materials for Coloration and Finishing. Wiley-Scrivener, USA, pp 303–356
24. Shahidi S, Wiener J (2012) Antibacterial Agents in Textile Industry. In: Bobbadala V (ed) Antimicrobial agents. InTech, Rijeka, pp 387–406
25. Romanò CL, Romanò D, De Vecchi E et al (2012) Antibacterial finishing reduces hospital textiles contamination. An experimental study. Eur Orthop Traumatol 3:177–182. https://doi.org/10.1007/s12570-012-0114-x
26. Kang CK, Kim SS, Kim S et al (2016) Antibacterial cotton fibers treated with silver nanoparticles and quaternary ammonium salts. Carbohydr Polym 151:1012–1018. https://doi.org/10.1016/j.carbpol.2016.06.043
27. Wang L, Wen X, Zhang X et al (2021) Durable antimicrobial cotton fabric fabricated by carboxymethyl chitosan and quaternary ammonium salts. Cellulose 28:5867–5879. https://doi.org/10.1007/s10570-021-03875-x
28. Abbasi AR, Morsali A (2012) US patent application no. 13/482,812
29. Abbasi AR, Akhbari K, Morsali A (2012) Dense coating of surface mounted CuBTC Metal-Organic Framework nanostructures on silk fibers, prepared by layer-by-layer method under ultrasound irradiation with antibacterial activity. Ultrason Sonochem 19:846–852
30. Hinestroza JP, Ochoa-puentes C, Sierra CA, Soto CY (2014) Antibacterial Activity Against Escherichia coli of Cu-BTC (MOF-199) Metal-Organic Framework Immobilized onto Cellulosic Fibers. J Appl Polym Sci 40815:1–5. https://doi.org/10.1002/app.40815
31. Jin B, Shen J, Peng R et al (2015) DMSO: An efficient catalyst for the cyclopropanation of C60, C70, SWNTs, and graphene through the bingel reaction. Ind Eng Chem Res 54:2879–2885. https://doi.org/10.1021/ie504918f
32. Abdelhameed RM, Emam HE, Rocha J, Silva AMS (2017) Cu-BTC metal-organic framework natural fabric composites for fuel purification. Fuel Process Technol 159:306–312. https://doi.org/10.1016/j.fuproc.2017.02.001
33. Emam HE, Darwesh OM, Abdelhameed RM (2018) In-growth metal organic framework/synthetic hybrids as antimicrobial fabrics and its toxicity. Colloids Surf B Biointerfaces 165:219–228. https://doi.org/10.1016/j.colsurfb.2018.02.028
34. Emam H, Abdelhameed RM, Darwesh OM (2020) Protective Cotton Textiles via Amalgamation of Cross-linked Zeolitic Imidazole Framework. Mater Interfaces. https://doi.org/10.1021/acs.iecr.0c01384
35. Tranchemontagne DJ, Hunt JR, Yaghi OM (2008) Room temperature synthesis of metal-organic frameworks: MOF-5, MOF-74, MOF-199, and IRMOF-0. Tetrahedron 64:8553–8557. https://doi.org/10.1016/j.tet.2008.06.036
36. Thi TVN, Luu CL, Hoang TC et al (2013) Synthesis of MOF-199 and application to CO2 adsorption. Adv Nat Sci Nanosci Nanotechnol 4:035016. https://doi.org/10.1088/2043-6262/4/3/035016
37. Bunge MA, Ruckart KN, Leavesley S et al (2015) Modification of fibers with nanostructures using reactive dye chemistry. Ind Eng Chem Res 54:3821–3827. https://doi.org/10.1021/acs.iecr.5b00089
38. Katz MJ, Brown ZJ, Colón YJ et al (2013) A facile synthesis of UiO-66, UiO-67 and their derivatives. Chem Commun 49:9449–9451. https://doi.org/10.1039/C3CC46105J
39. Lu L, Hu C, Zhu Y et al (2018) Multi-functional finishing of cotton fabrics by water-based layer-by-layer assembly of metal–organic framework. Cellulose 25:4223–4238. https://doi.org/10.1007/s10570-018-1838-8
40. Shen M, Ye X, Forghani F et al (2020) Antibacterial applications of metal – organic frameworks and their composites. Compr Rev

Food Sci Food Saf 19:1397–1419. https://doi.org/10.1111/1541-4337.12515
41. Zhou S, Gao J, Zhu J et al (2020) Self-cleaning, antibacterial mixed matrix membranes enabled by photocatalyst Ti-MOFs for efficient dye removal. J Memb Sci 610:118219. https://doi.org/10.1016/j.memsci.2020.118219
42. Calderón-Vergara LA, Ovalle-Serrano SA, Blanco-Tirado C, Combariza MY (2020) Influence of post-oxidation reactions on the physicochemical properties of TEMPO-oxidized cellulose nanofibers before and after amidation. Cellulose 27:1273–1288. https://doi.org/10.1007/s10570-019-02849-4
43. Ovalle-Serrano SA, Díaz-Serrano LA, Hong C et al (2020) Synthesis of cellulose nanofiber hydrogels from fique tow and Ag nanoparticles. Cellulose 27:9947–9961. https://doi.org/10.1007/s10570-020-03527-6
44. Fu H, Ou P, Zhu J et al (2019) Enhanced Protein Adsorption in Fibrous Substrates Treated with Zeolitic Imidazolate Framework-8 (ZIF-8) Nanoparticles. ACS Appl Nano Mater 2:7626–7636. https://doi.org/10.1021/acsanm.9b01717
45. Zhang XF, Feng Y, Wang Z et al (2018) Fabrication of cellulose nanofibrils/UiO-66-NH2 composite membrane for CO2/N2 separation. J Memb Sci 568:10–16. https://doi.org/10.1016/j.memsci.2018.09.055
46. da Silva PD, Montanari S, Vignon MR (2003) TEMPO-Mediated Oxidation of Cellulose III. Biomacromol 4:1417–1425. https://doi.org/10.1021/bm034144s
47. Vellingiri K, Deep A, Kim KH et al (2017) The sensitive detection of formaldehyde in aqueous media using zirconium-based metal organic frameworks. Sens Actuators B Chem 241:938–948. https://doi.org/10.1016/j.snb.2016.11.017
48. Prestipino C, Regli L, Vitillo JG et al (2006) Local structure of framework Cu(II) in HKUST-1 metallorganic framework: Spectroscopic characterization upon activation and interaction with adsorbates. Chem Mater 18:1337–1346. https://doi.org/10.1021/cm052191g
49. Kandiah M, Nilsen MH, Usseglio S et al (2010) Synthesis and Stability of Tagged UiO-66 Zr-MOFs. Chem Mater 22:6632–6640. https://doi.org/10.1021/cm102601v
50. Cao Y, Zhang H, Song F et al (2018) UiO-66-NH2/GO composite: Synthesis, characterization and CO2 adsorption performance. Materials 11:1–15. https://doi.org/10.3390/ma11040589
51. Nanda AK, Matyjaszewski K (2003) Effect of [PMDETA]/[Cu(I)] ratio, monomer, solvent, counterion, ligand, and alkyl bromide on the activation rate constants in atom transfer radical polymerization. Macromolecules 36:1487–1493. https://doi.org/10.1021/ma0340107
52. Saito T, Isogai A (2004) TEMPO-mediated oxidation of native cellulose. The effect of oxidation conditions on chemical and crystal structures of the water-insoluble fractions. Biomacromol 5:1983–1989. https://doi.org/10.1021/bm0497769
53. Isogai A, Saito T, Fukuzumi H (2011) TEMPO-oxidized cellulose nanofibers. Nanoscale 3:71–85. https://doi.org/10.1039/c0nr00583e
54. Van Nguyen Thi T, Luu CL, Hoang TC et al (2013) Synthesis of MOF-199 and application to CO2 adsorption. Adv Nat Sci Nanosci Nanotechnol 4:35016. https://doi.org/10.1088/2043-6262/4/3/035016
55. Moulder F, Wagner C, Riggs W, Davis L (1979) Handbook of X-ray Photoelectron Spectroscopy. Perkin-Elmer Corporation
56. Hamisu AM, Ariffin A, Wibowo AC (2020) Cation exchange in metal-organic frameworks (MOFs): The hard-soft acid-base (HSAB) principle appraisal. Inorganica Chim Acta 511:119801. https://doi.org/10.1016/j.ica.2020.119801
57. Ardila-Suárez C, Rodríguez-Pereira J, Baldovino-Medrano VG, Ramírez-Caballero GE (2019) An analysis of the effect of zirconium precursors of MOF-808 on its thermal stability, and structural and surface properties. ChemRxiv 21:1407–1415. https://doi.org/10.1039/c8ce01722k
58. Schelling M, Kim M, Otal E, Hinestroza J (2018) Decoration of Cotton Fibers with a Water-Stable Metal-Organic Framework (UiO-66) for the Decomposition and Enhanced Adsorption of Micropollutants in Water. Bioengineering 5:14. https://doi.org/10.3390/bioengineering5010014
59. Ansel HC, Norred WP, Roth IL (1969) Antimicrobial activity of dimethyl sulfoxide against Escherichia coli, Pseudomonas aeruginosa, and Bacillus megaterium. J Pharm Sci 58:836–839. https://doi.org/10.1002/jps.2600580708
60. da Silva PM, Sierra-Avila CA, Hinestroza JP (2012) *In situ* synthesis of a Cu-BTC metal-organic framework (MOF 199) onto cellulosic fibrous substrates: Cotton. Cellulose 19:1771–1779. https://doi.org/10.1007/s10570-012-9752-y
61. Wang C, Qian X, An X (2015) *In situ* green preparation and antibacterial activity of copper-based metal–organic frameworks/cellulose fibers (HKUST-1/CF) composite. Cellulose 22:3789–3797. https://doi.org/10.1007/s10570-015-0754-4
62. Mortada B, Matar TA, Sakaya A et al (2017) Postmetalated Zirconium Metal Organic Frameworks as a Highly Potent Bactericide. Inorg Chem 56:4739–4744. https://doi.org/10.1021/acs.inorgchem.7b00429
63. Mao K, Zhu Y, Rong J et al (2021) Rugby-ball like Ag modified zirconium porphyrin metal–organic frameworks nanohybrid for antimicrobial activity: Synergistic effect for significantly enhancing photoactivation capacity. Colloids Surf A Physicochem Eng Asp 611:125888. https://doi.org/10.1016/j.colsurfa.2020.125888
64. Gupta A, Mumtaz S, Li C-H et al (2019) Combatting antibiotic-resistant bacteria using nanomaterials. Chem Soc Rev 48:415–427. https://doi.org/10.1039/C7CS00748E
65. Abdelhameed RM, Rehan M, Emam HE (2018) Figuration of Zr-based MOF@cotton fabric composite for potential kidney application. Carbohydr Polym 195:460–467. https://doi.org/10.1016/j.carbpol.2018.04.122